Nodeless superconductivity in the noncentrosymmetric compound ThIrSi

D. Tay, T. Shang, Priscila F. S. Rosa, F. B. Santos, J. D. Thompson, Z. Fisk, H.-R. Ott, and T. Shiroka

Phys. Rev. B **107**, 064507 — Published 14 February 2023

DOI: 10.1103/PhysRevB.107.064507

Nodeless superconductivity in the noncentrosymmetric ThIrSi compound

D. Tay,[1] T. Shang,[2,*] Priscila F. S. Rosa,[3] F. B. Santos,[3,4] J. D. Thompson,[3] Z. Fisk,[5] H.-R. Ott,[1] and T. Shiroka[1,6,†]

[1]*Laboratorium für Festkörperphysik, ETH Zürich, CH-8093 Zürich, Switzerland*
[2]*Key Laboratory of Polar Materials and Devices (MOE), School of Physics and Electronic Science, East China Normal University, Shanghai 200241, China*
[3]*Los Alamos National Laboratory, Los Alamos, NM 87545, USA*
[4]*Escola de Engenharia de Lorena, Universidade de São Paulo (EEL-USP), Materials Engineering Department (Demar), Lorena, São Paulo, Brazil*
[5]*Department of Physics and Astronomy, University of California at Irvine, Irvine, California 92697, USA*
[6]*Laboratory for Muon-Spin Spectroscopy, Paul Scherrer Institut, Villigen PSI, Switzerland*

The ThIrSi superconductor, with $T_c = 6.5$ K, is expected to show unusual features in view of its noncentrosymmetric structure and the presence of heavy elements featuring a sizable spin-orbit coupling. Here, we report a comprehensive study of its electronic properties by means of local-probe techniques: muon-spin rotation and relaxation (SR) and nuclear magnetic resonance (NMR). Both the superfluid density $\rho_{sc}(T)$ (determined via transverse-field SR) and the spin-lattice relaxation rate $T_1^{-1}(T)$ (determined via NMR) suggest a nodeless superconductivity. Furthermore, the absence of spontaneous magnetic fields below T_c, as evinced from zero-field SR measurements, indicates a preserved time-reversal symmetry in the superconducting state of ThIrSi. Temperature-dependent upper critical fields as well as field-dependent superconducting muon-spin relaxations suggest the presence of multiple superconducting gaps in ThIrSi.

I. INTRODUCTION

Superconductors whose crystal structures lack an inversion center are known as noncentrosymmetric superconductors (NCSCs) and represent appealing systems for investigating unconventional- and topological superconductivity (SC) [1–11]. Since in NCSCs parity is not a good quantum number, this allows for the presence of an antisymmetric spin-orbit coupling (ASOC), which lifts the degeneracy of the conduction-electron bands and splits the Fermi surface. Consequently, both intra- and inter-band Cooper pairs can be formed, resulting in an admixture of spin-singlet and spin-triplet pairings [1, 2]. Unfortunately, in actual NCSCs systems, while some of them, like Li_2Pt_3B, do indeed exhibit spin-triplet pairing [12], many others do not. For instance, previous studies on some highly-anticipated NCSCs, such as Re_7B_3[13], W_3Al_2C [14], Mo_3Al_2C[15] and NbReSi [16], reveal no spin-triplet superconductivity, despite sizable SOC interactions.

However, spin-triplet superconductivity is not the only possible outcome of ASOC. Since ASOC causes the splitting of the Fermi surface, it may conceivably also constitute a generic mechanism to achieve two-band superconductivity. The latter has been a prominent issue following the discovery of superconductivity in MgB_2 [17], where the presence of strongly anisotropic σ-bands and isotropic π-bands gives rise to two-band SC [18]. Since then, efforts have been made to investigate and understand two-band superconductivity also in other materials. Among the most promising two-band superconductors are the sesquicarbides, which comprise the La_2C_3 and Y_2C_3 NCSCs. NMR [19] and SR studies [20] of sesquicarbides provide hints of multigap superconductivity, with both bands proposed to be of s-type, thus implying a two-band $(s+s)$ model. On the other hand, heat-capacity-[21] and tunneling break-junction measurements [22] on the same compounds indicate a conventional s-type single-band superconductivity. Hence, the question of whether the sesquicarbides can be described by a two-band- or by a single-band model is still controversial. Such controversy is largely due to the fact that, in the proposed two-band model of sesquicarbides, the average gap value is close to the BCS theoretical value $2\Delta/k_B T_c = 3.52$, making it experimentally challenging to distinguish between the two cases. A two-band model was also used to describe the SR results in NbReSi [16], where again the two bands have similar gap values, so the additional band does not significantly affect the physical properties of this system. As for ThIrSi, object of the current study, previous DFT calculations have shown the presence of multiple bands near the Fermi surface [23], hence strongly suggesting that also ThIrSi may exhibit multiband superconductivity.

Ternary equiatomic transition-metal silicides of the ThTSi family, with T = Co, Ir, Ni, and Pt, have been known since the eighties [24–27]. The original focus was on their synthesis and structural characterization, followed by the detection of superconductivity through electrical resistivity measurements [25, 26]. Later on, these first results were complemented by more detailed specific-heat and contact-point spectroscopy investigations [27]. In recent years, interest in ternary transition-metal silicides was re-ignited by the discovery of spin-triplet SC in LaT(Si,Ge) Weyl nodal-line semimetals, whose time-reversal symmetry (TRS) is broken in the superconducting state [28]. Yet, less is known about their thorium conterpart.

Here, we revisit the ThTSi family in more detail and report about a comprehensive study of superconductivity in ThIrSi by means of SQUID magnetometry, SR, and NMR. Below we show that ThIrSi is an unambiguous example of a NCSC that exhibits nodeless superconductivity. All our results show features typical of fully-gapped superconductors. The temperature-dependent superfluid density is compatible with either a single-band s-wave model with $\Delta/k_B T_c = 2.10(5)$, or with a two-band $(s+s)$ model, with $\Delta_\alpha = 1.90(5) k_B T_c$ and $\Delta_\beta = 2.20(5) k_B T_c$. This uncertainty about multiband nature is resolved by measurements of temperature-dependent upper critical fields and of field-dependent muon-spin relaxation in the SC state, both of which clearly suggest multiband superconductivity in ThIrSi.

II. EXPERIMENTAL DETAILS

Polycrystalline ThIrSi samples were prepared by arc melting stoichiometric amounts of Th (99.9%), Ir (99.95%), and Si (99.9999%) in a water-cooled copper hearth under argon atmosphere. No weight loss was observed during the melting process. The obtained arc-melted button was

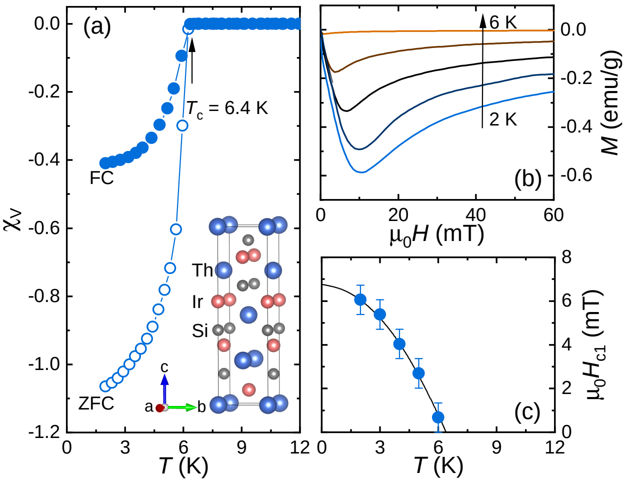

FIG. 1. (a) Temperature dependence of the magnetic susceptibility $\chi_V(T)$, in SI units, measured at 1 mT. The inset shows the crystal structure of ThIrSi. (b) Field-dependent magnetization curves collected at various temperatures after cooling the sample in zero field. (c) Lower critical fields H_{c1} vs. temperature. Solid lines are fits to $\mu_0H_{c1}(T) = \mu_0H_{c1}(0)[1-(T/T_c)^2]$. For each temperature, H_{c1} was determined as the value where $M(H)$ starts deviating from linearity. Both magnetic susceptibility values and lower critical fields were corrected by accounting for the demagnetization factor.

flipped over and melted repeatedly to ensure homogeneity. The as-cast samples were then wrapped in a tantalum foil and annealed in a quartz tube under vacuum at 1000°C for one week. The crystal structure of the resulting alloy was checked at ambient temperature by means of powder x-ray diffraction using Cu Kα radiation. This confirmed a non-centrosymmetric tetragonal structure of LaPtSi-type with space group $I4_1md$ (No. 109) [see inset in Fig. 1(a)]. Magnetization measurements were performed on a Quantum Design magnetic property measurement system.

The bulk SR measurements were carried out at the general-purpose surface-muon instrument (GPS) of the Swiss muon source at Paul Scherrer Institut, Villigen, Switzerland. In this study, we performed two types of experiments: transverse-field (TF)-, and zero-field (ZF)-SR measurements. As to the former, it allowed us to determine the temperature evolution of the superfluid density. As to the latter, we aimed at searching for a possible breaking of time-reversal symmetry in the superconducting state of ThIrSi. To avoid the effects of stray magnetic fields during the ZF-SR measurements, all magnets were preliminarily degaussed. The SR spectra were collected upon sample heating and then analyzed by means of the `musrfit` software package [29].

The ^{29}Si NMR measurements, including line shapes and spin-lattice relaxation times, were performed on ThIrSi in powder form in a magnetic field of 3 T. The NMR reference frequency ν_0 was determined from the ^{29}Si resonance signal in tetramethylsilane (TMS). Subsequently, the ^{29}Si NMR shifts were calculated with respect to ν_0. To cover the 2 to 300 K temperature range we used a continuous-flow CF-1200 cryostat by Oxford Instruments, with temperatures below 4.2 K being achieved under pumped ^{4}He conditions. The ^{29}Si NMR signal was detected by means of a standard spin-echo sequence consisting of $\pi/2$ and π pulses of 3 and 6 s, with recycling delays ranging from 1 to 60 s in the 2–300 K temperature range. The line shapes were obtained via fast Fourier transform (FFT) of the echo signal. Spin-lattice relaxation times T_1 were measured via the inversion-recovery method, using a π–$\pi/2$–π pulse sequence. In all the measurements, phase cycling was used to systematically minimize the presence of artifacts.

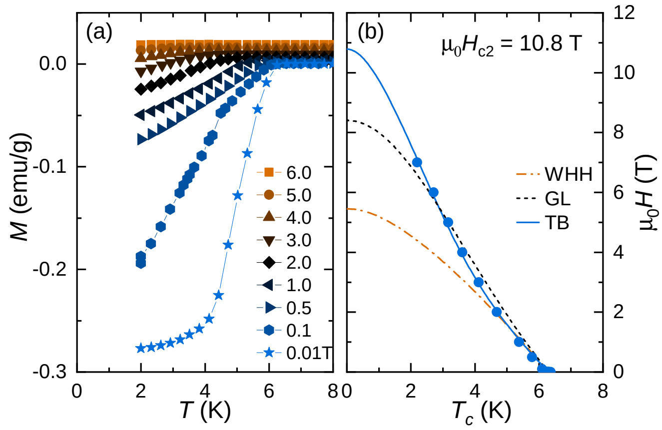

FIG. 2. (a) Temperature-dependent magnetization curves $M(T,H)$ for various applied magnetic fields. (b) Upper critical fields H_{c2} vs. transition temperature T_c. The dash-dotted-, dotted-, and solid lines represent fits to the WHH, GL, and TB models, respectively.

III. RESULTS AND DISCUSSION

A. Magnetization measurements

The bulk superconductivity of ThIrSi was first characterized by magnetic-susceptibility measurements, using both field-cooled (FC) and zero-field-cooled (ZFC) protocols in an applied field of 1 mT. As shown in Fig. 1(a), a clear diamagnetic signal appears below the superconducting transition at $T_c = 6.4$ K. A rather sharp transition (with a $\Delta T \sim 0.4$ K) indicates a good sample quality. After accounting for the demagnetizing effects, we find an almost 100% superconducting shielding fraction, suggestive of bulk SC, definitely confirmed by SR measurements (see below).

To determine the lower critical field H_{c1}, the field-dependent magnetization $M(H)$ of ThIrSi was measured at various temperatures up to 6 K. Figure 1(b) shows the $M(H)$ curves at various temperatures. The estimated H_{c1} values as a function of temperature (accounting also for a demagnetization factor) are summarized in Fig. 1(c). The solid lines are fits to $\mu_0H_{c1}(T) = \mu_0H_{c1}(0)[1-(T/T_c)^2]$ and yield a lower critical field $\mu_0H_{c1}(0) = 6.8(1)$ mT for ThIrSi.

We also performed temperature-dependent magnetization measurements $M(T,H)$ at various applied magnetic fields up to 7 T. For each field, T_c was determined from the intersection of two straight lines drawn on the normal and transition region. As shown in Fig. 2(a), upon increasing the magnetic field, the superconducting transition in $M(T)$ becomes broader and shifts to lower temperatures. Figure 2(b) summarizes the superconducting transition temperature T_c vs. the applied magnetic field, as identified from the $M(H,T)$ data of ThIrSi. The $H_{c2}(T)$ was analyzed by means of Ginzburg-Landau (GL) [30], Werthamer-Helfand-Hohenberg (WHH) [31], and two-band (TB) models [32]. As shown in Fig. 2, both the GL- and WHH models show large deviations, leading to underestimated H_{c2} values at zero temperature. Such discrepancy most likely hints at multiple superconducting gaps in ThIrSi, as evidenced also by the positive curvature of $H_{c2}(T)$ at low fields, a typical feature of multigap superconductors, as e.g., MgB_2 [33, 34] or $Lu_2Fe_3Si_5$ [35]. As shown in Fig. 2(b), around $\mu_0H \sim$2-3 T, $H_{c2}(T)$ undergoes a clear change in curvature. The remarkable agreement of the TB model with the experimental data across the full temperature range is obvious and it allows us to determine $\mu_0H_{c2}(0) = 10.8(2)$ T and

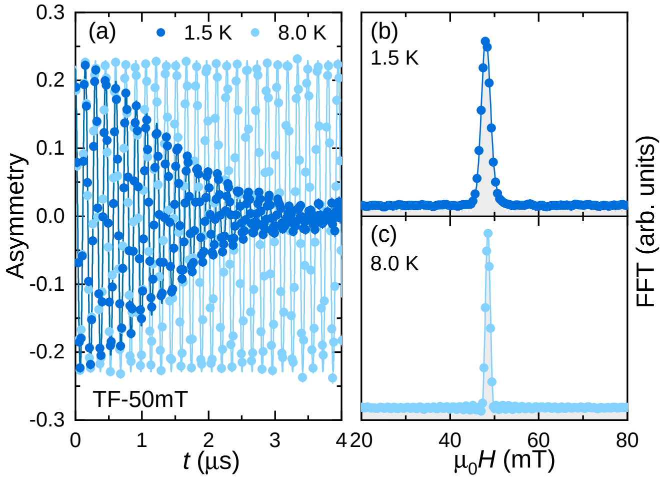

FIG. 3. (a) TF-SR spectra collected in an applied field of 50 mT in both the superconducting- and normal states for ThIrSi. The real part of the fast Fourier transform of SR spectra is shown in (b) and (c) for 1.5 K and 8.0 K, respectively. Solid lines are fits to Eq. (1). The TF-200 mT SR spectra shows similar features.

$\xi(0) = 5.52(5)$ nm. The lower critical field μ_0H_{c1} is related to the magnetic penetration depth λ and the coherence length ξ via $\mu_0H_{c1} = (\Phi_0/4\pi\lambda^2)[\ln(\kappa)+0.5]$, where $\kappa = \lambda/\xi$ is the GL parameter [36]. By using $\mu_0H_{c1} = 6.8(1)$ mT and $\mu_0H_{c2} = 10.8(2)$ T, the resulting magnetic penetration depth $\lambda_{GL} = 333(3)$ nm, is comparable to the experimental value 370(2) nm we determine from TF-SR data (see below). The large GL parameter, $\kappa \sim 60$, clearly indicates that ThIrSi is a type-II superconductor. Lastly, when we compare H_{c2} to the Pauli limit H_P, given by $\mu_0H_P = \frac{\Delta_0}{\sqrt{2}\mu_B} \approx 1.86\,[\mathrm{T/K}]\,T_c$, we note that a T_c of 6.4 K corresponds to a μ_0H_P of 11.9 T. Hence, the observed superconductivity in ThIrSi is well below the Pauli limit, as expected of a conventional nodeless superconductor.

B. SR study

To investigate the superconducting pairing of ThIrSi, we carried out systematic temperature-dependent TF-SR measurements in two magnetic fields: 50 and 200 mT. After cooling the sample in a transverse field, the TF-SR spectra were collected upon heating. Representative datasets for TF-50 mT, taken in the superconducting- and normal states of ThIrSi, are shown in Fig. 3, with the TF-200 mT SR spectra showing similar features. In the normal state, the SR asymmetry shows essentially no damping, thus reflecting a uniform field distribution. Conversely, in the superconducting state (here, at 1.5 K), the significantly enhanced damping reflects the inhomogeneous field distribution due to the development of a flux-line lattice (FLL) [37–39]. The broadening of the field distribution in the SC phase is clearly visible in Fig. 3(b) vs. Fig. 3(c), where the fast-Fourier-transform (FFT) spectra of the corresponding TF-50 mT SR data are shown. To properly describe the field distribution, the time-dependent TF-SR asymmetry was modeled using:

$$A_{TF}(t) = A_s\cos(\gamma_\mu B_s t+\phi)e^{-\sigma^2t^2/2} + A_{bg}\cos(\gamma_\mu B_{bg}t+\phi). \quad (1)$$

Here A_s (98%), A_{bg} (2%) and B_s, B_{bg} are the initial asymmetries and local fields sensed by implanted muons in the sample and sample holder, $\gamma_\mu/2\pi = 135.53$ MHz/T is the muon gyromagnetic ratio, ϕ is a shared initial phase, and σ is a Gaussian relaxation rate reflecting the field distribution inside the sample. The derived σ are small and temperature-

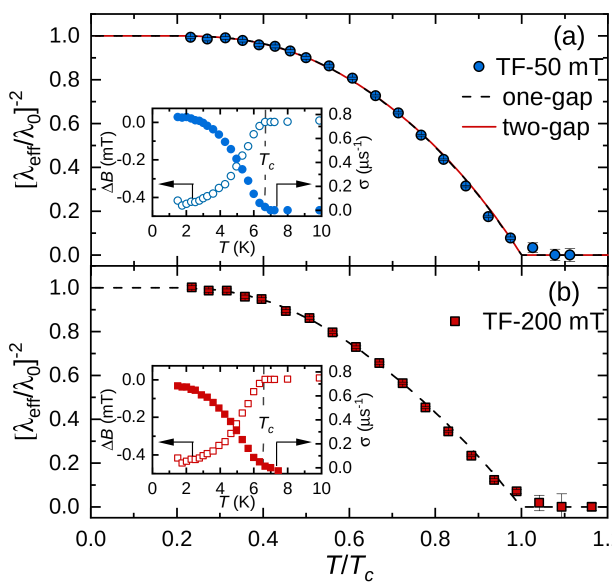

FIG. 4. Superfluid density vs temperature, as determined from TF-SR measurements in an applied magnetic field of 50 mT (a) and 200 mT (b). The insets show the diamagnetic shift $\Delta B(T)$(left-axis) and muon-spin relaxation rates $\sigma(T)$ (right-axis). Here, $\Delta B = B_s - B_{appl.}$, where $B_{appl.} = 50$ or 200 mT. The dashed- and solid lines represent fits to a fully-gapped model with a single gap and two gaps, respectively. The fit parameters are listed in Table I.

independent in the normal state, but below T_c they start to increase due to the onset of FLL and the increased superfluid density. Simultaneously, a diamagnetic shift ΔB appears below T_c (see inset in Fig. 4). In the superconducting state, σ includes contributions from both the FLL (σ_{sc}) and a smaller, temperature-independent relaxation, due to the nuclear moments (σ_n). Considering the constant nuclear relaxation rate in the narrow temperature range investigated here, confirmed also by ZF-SR measurements (see below), the superconducting Gaussian relaxation rate can be extracted using $\sigma_{sc} = \sqrt{\sigma_{eff}^2 - \sigma_n^2}$.

Since σ_{sc} is directly related to the effective magnetic penetration depth and, thus, to the superfluid density, the superconducting gap and its symmetry can be investigated by measuring the temperature-dependent σ_{sc}. Then, the effective magnetic penetration depth λ_{eff} can be obtained by using $\sigma_{sc}^2(T)/\gamma_\mu^2 = 0.00371\Phi_0^2/\lambda_{eff}^4(T)$ [36, 40].

The normalized inverse-square of the effective magnetic penetration depth [proportional to the superfluid density, i.e., $\lambda_{eff}^{-2}(T) \propto \rho_{sc}(T)$] vs. the reduced temperature T/T_c is presented in Fig. 4(a) and 4(b) for TF-50 mT and TF-200 mT SR spectra, respectively. In both cases, the superfluid densities are temperature invariant below $1/3T_c$, thus indicating the absence of low-energy excitations and, hence, a fully-gapped superconducting state in ThIrSi. Such nodeless SC is also confirmed by NMR measurements (see below). Consequently, the superfluid density $\rho_{sc}(T)$ was analyzed by means of a fully-gapped s-wave model:

$$\rho_{sc}(T) = \frac{\lambda_{eff}^{-2}(T)}{\lambda_0^{-2}} = 1 + 2\int_{\Delta(T)}^{\infty} \frac{\partial f}{\partial E} \frac{E dE}{\sqrt{E^2 - \Delta^2(T)}}. \quad (2)$$

Here, $f = (1 + e^{E/k_B T})^{-1}$ is the Fermi function; $\Delta(T)$ is the superconducting-gap function, assumed to follow $\Delta(T) = \Delta_0 \tanh\{1.82[1.018(T_c/T - 1)]^{0.51}\}$ [41, 42]; λ_0 and Δ_0 are the magnetic penetration depth and the superconducting gap at 0 K, respectively. As shown by the solid lines in Fig. 4, the s-wave model describes $\rho_{sc}(T)$ very well across the entire temperature range with the fit parameters: $\Delta_0 = 2.10(5)$ and $1.90(5)\, k_B T_c$, and $\lambda_0 = 370(2)$ and 397(2) nm for TF-50 mT and TF-200 mT SR spectra, respectively.

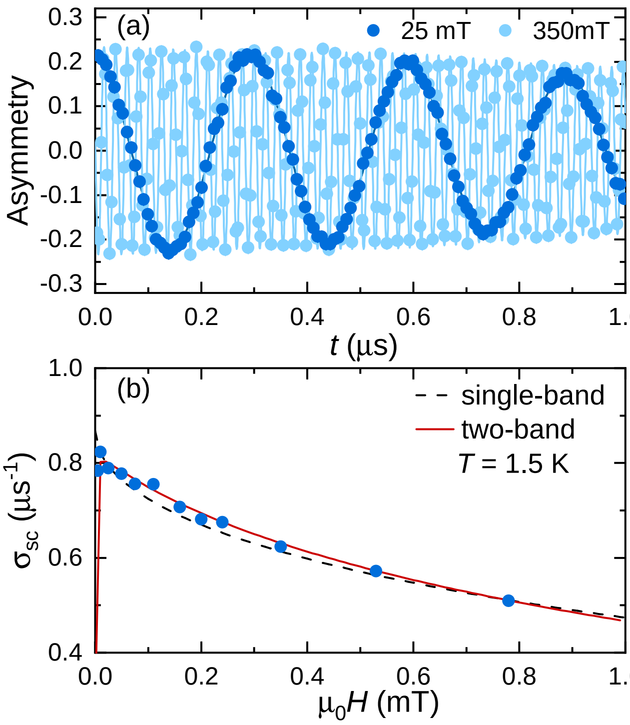

FIG. 5. (a) TF-SR time spectra measured in the superconducting state of ThIrSi (at $T = 1.5$ K) in a field of 25 and 350 mT. (b) Field-dependent superconducting Gaussian relaxation rate $\sigma_{sc}(H)$. Dashed- and solid lines represent fits to the single- and two-band models, respectively. The goodness-of-fit values are $\chi_r^2 = 3.2$ (two-band model) and 8.4 (single-band model). In both cases, data below H_{c1} were excluded when evaluating χ_r^2.

Since the $H_{c2}(T)$ data (see Fig. 2) show some features of multigap SC, we analyzed the superfluid density also with the so-called α-model. In this case, the superfluid density can be described by $\rho_{sc}(T) = \alpha \rho_{sc}^{\Delta^\alpha}(T) + (1-\alpha)\rho_{sc}^{\Delta^\beta}(T)$, where $\rho_{sc}^{\Delta^\alpha}$ and $\rho_{sc}^{\Delta^\beta}$ are the superfluid densities related to the first (Δ^α) and second (Δ^β) gap, and α is a relative weight. For each gap, $\rho_{sc}(T)$ is given by Eq. (2). As shown by the solid line in Fig. 4(a), by using the same λ_0 value and by fixing w to 0.3 (as derived from the field-dependent TF-SR measurements reported below), the resulting gap values are $\Delta^\alpha = 1.90(5)\, k_B T_c$ and $\Delta^\beta = 2.20(5)\, k_B T_c$. However, as shown in Fig. 4, the two-gap fit (solid line) is virtually indistinguishable from the one-gap fit (dashed line).

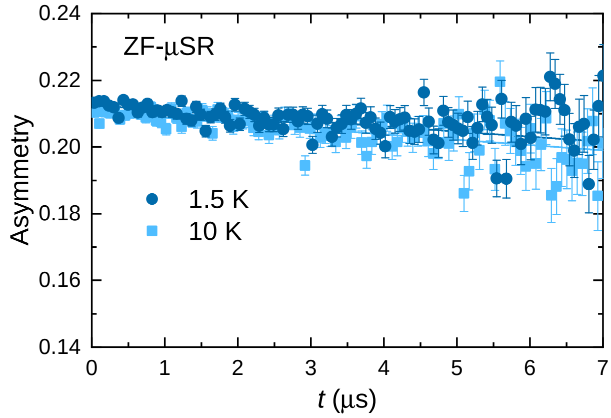

FIG. 6. ZF-SR spectra collected in the superconducting- (1.5 K) and the normal (10 K) states of ThIrSi. The practically overlapping datasets indicate the absence of TRS breaking, whose occurrence would have resulted in a stronger decay in the 0.3-K case.

This circumstance might be attributed to the relatively small weight of the second gap, as well as to the comparable gap-energy sizes, both factors which make it difficult to discriminate between a single- and a two-gap superconductor based on the temperature-dependent superfluid density alone. In this case, measurements of the field-dependent superconducting Gaussian relaxation rate $\sigma_{sc}(H)$ provides suitable alternatives to disentangle the two cases, since the respective datasets are expected to show distinct field responses in a two-gap vs. a single-gap superconductor [16, 43]. Based on this, to ascertain the possibility of a multigap SC in ThIrSi, we performed TF-SR measurements at base temperature (1.5 K) at different applied fields, up to 780 mT. Figure 5(a) shows two representative TF-SR datasets, collected at 25 and 350 mT, with the spectra in other applied fields showing similar features. Also in this case, we fitted the data by means of Eq. (1), with the resulting superconducting Gaussian relaxation rates σ_{sc} vs the applied magnetic field being summarized in Fig. 5(b). $\sigma_{sc}(H)$ was analyzed using both a single- and a two-band model. In the latter case, each band is characterized by its own superconducting coherence length [i.e., $\xi_1(0)$ and $\xi_2(0)$], while a weight w accounts for the contribution of the first band [$\xi_1(0)$] to the total superfluid density, akin to the two-gap model in Fig. 4 [44, 45]. As shown in Fig. 5(b), the two-band model (solid line) shows a better agreement with the data, here reflected in a smaller χ_r^2 value, and it yields these best-fit parameters: $w = 0.3$, $\xi_1(0) = 12.0$ nm, $\xi_2(0) = 5.4$ nm, and $\lambda_0 = 357$ nm. The derived λ_0 is consistent with that obtained from the $\rho_{sc}(T)$ analysis in Fig. 4 (370 nm). Finally, the upper critical field of 11.2 T, calculated from the coherence length of the second band $\xi_2(0)$, is comparable with the H_{c2} value determined from the $M(T, H)$ data (see Fig. 2). As for the first band, the critical field of 2.3 T, calculated from $\xi_1(0)$, is in good agreement with the field value where $H_{c2}(T)$ changes its slope [see Fig. 2(b)]. Note that, in case of the NMR measurements, here performed in a magnetic field of 3 T, the required high field can suppress the smaller gap. As a consequence, the material is expected to appear more like a single-gap superconductor.

We also performed zero-field (ZF-) SR measurements in the normal- and superconducting states of ThIrSi, in order to reveal a possible breaking of the time-reversal symmetry (TRS), in turn implying an unconventional SC. As shown in

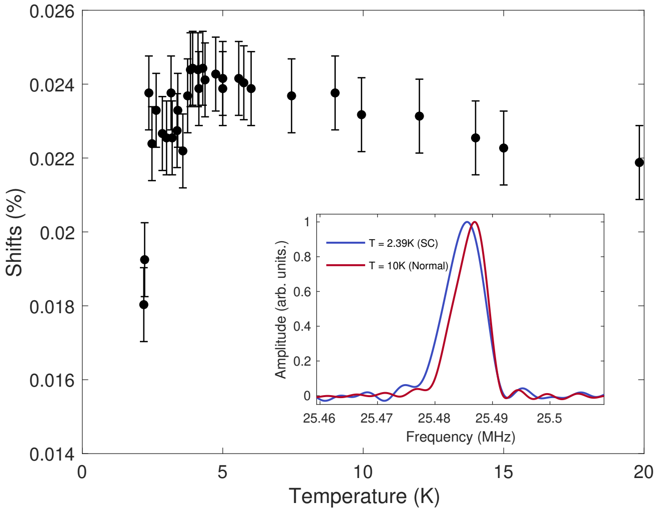

FIG. 7. Evolution of the ^{29}Si NMR shift with temperature. As typical for *s*-wave superconductors, the shift decreases below T_c. Inset: Representative ^{29}Si NMR line shapes in the superconducting- and the normal state, collected in a magnetic field of 3 T.

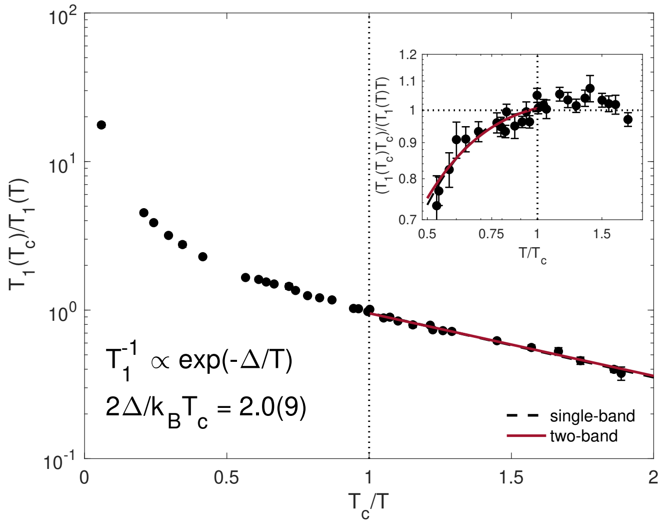

FIG. 8. Normalized NMR relaxation rate vs the scaled temperature (measured at $\mu_0 H = 3\,\mathrm{T}$). The decay follows an exponential law, $T_1^{-1} \propto \exp(-\Delta/k_\mathrm{B}T)$, typical of *s*-wave superconductors with a fixed gap Δ. Inset: Scaled Korringa product vs the scaled temperature. In both cases, the two-band fit (solid line) is hardly distinguishable from the single-band fit (dashed line), most likely reflecting the suppression of the smaller gap by the magnetic field.

Fig. 6, neither coherent oscillations nor fast decays could be identified in the spectra collected below- (1.5 K) and above T_c (10 K), thus excluding any type of magnetic order or fluctuations. In nonmagnetic materials, in the absence of applied fields, the depolarization of muon spins is mainly determined by the randomly oriented nuclear magnetic moments. In ThIrSi, the depolarization shown in Fig. 6 is more consistent with a Lorentzian decay. This suggests that the internal fields sensed by the implanted muons arise from the diluted (and tiny) nuclear moments present in ThIrSi. Thus, the solid lines in Fig. 6 are fits to a Lorentzian Kubo-Toyabe relaxation function $A(t) = A_\mathrm{s}[\frac{1}{3}+\frac{2}{3}(1-\Lambda_\mathrm{ZF}t)\mathrm{e}^{-\Lambda_\mathrm{ZF}t}]+A_\mathrm{bg}$. Here, A_s and A_bg are the same as in the TF-SR case [see Eq. (1)], while Λ_ZF represents the ZF Lorentzian relaxation rate. The derived relaxation rates in the normal- and the superconducting state are almost identical, i.e., $\Lambda_\mathrm{ZF} = 0.0057(7)\,\mathrm{s}^{-1}$ at 1.5 K and $\Lambda_\mathrm{ZF} = 0.0060(8)\,\mathrm{s}^{-1}$ at 10 K, here reflected in overlapping datasets. The lack of an additional SR relaxation below T_c excludes a possible TRS breaking in the superconducting state of ThIrSi. As we show below, the conventional nature of SC in ThIrSi is further supported by the exponential dependence of the NMR relaxation rate and by a clear drop in the NMR shift below T_c.

C. ^{29}Si NMR study

From the basic theory of NMR in superconducting materials (see, e.g., Ref. 46), it is known that conventional BCS superconductors exhibit three key signatures below T_c:

a. A reduced Knight shift K with respect to the normal-state value.
b. An exponential decrease of the relaxation rate $T_1^{-1}(T)$.
c. The appearance of a Hebel-Slichter (HS) coherence peak in the Korringa product $(T_1T)^{-1}$ just below T_c.

In ThIrSi, the decreasing Knight shift below T_c is clearly evident in Fig. 7, while the exponential decrease of $T^{-1}(T)$ below T_c is made obvious by the semilogarithmic scale in Fig. 8. The only missing signature is the Hebel-Slichter coherence peak, which is conspicuously absent in Fig. 8 (see inset). However, we recall that the Hebel-Slichter peak is suppressed also in other conventional noncentrosymmetric superconductors, such as NbReSi [16] and W_3Al_2C [14], which also are fully gapped. A comparison of $1/T_1T$ vs T in different NCSCs is given in our previous paper [14]. It appears that, experimentally the Hebel-Slichter peak is either completely absent or strongly suppressed in the NCSCs studied. Hence, it is not surprising that we do not observe this feature in ThIrSi either. Furthermore, the two main signatures of nodal (triplet) superconductivity [1], namely a power-law dependence of relaxation rates and a temperature-independent Knight shift below T_c, are clearly missing in our case. Hence, in spite of the lack of an HS peak, nodeless superconductivity remains the most convincing scenario compatible with our NMR data.

Next, we move on to discuss the details of the gap structure found via NMR. As can be seen in Fig. 8, the NMR relaxation rate follows a single-exponential law, here depicted by the dashed line. However, the gap resulting from the single-exponential fit is $2\Delta/k_\mathrm{B}T_c = 2.0(9)$, which is significantly lower than that predicted by the BCS theory, i.e., $2\Delta/k_\mathrm{B}T_c = 3.5$. We attempted to fit the data using a two-exponential function, but the second exponential does not change the result. The value of the main gap is still $2\Delta_a/k_\mathrm{B}T_c = 2.0(9)$ (within experimental error), while the second exponential has a negligibly small weight. Although apparently NMR seems to exclude the possibility of a two-gap superconductivity, it is quite likely that the magnetic field required for the NMR experiments might suppress the smaller gap.

D. Discussion

In ThIrSi, we find that the datasets resulting from three different techniques: i.e., magnetometry, SR, and NMR, agree in indicating a fully-gapped singlet superconducting state. However, the situation is less clear with respect to the char-

Table I. Superconducting gap values of ThIrSi compared to those of Y_2C_3 and La_2C_3, as obtained from NMR and SR measurements. The NMR T_c and Δ values refer to the 3-T magnetic field. The experimental uncertainties are of the order of the last digit.

Compound	Technique	$2\Delta_\alpha/k_B T_c$	$2\Delta_\beta/k_B T_c$	α/β
ThIrSi	SR	4.4	3.8	0.3/0.7
ThIrSi	NMR	2.0	NA	NA
Y_2C_3 [20]	SR	4.9	1.1	0.86/0.14
Y_2C_3 [19]	NMR	5.0	2.0	0.75/0.25
La_2C_3 [20]	SR	5.6	1.3	0.38/0.62

acteristics of the s-wave type pairing, i.e., whether it involves quasiparticles in a one- or two-band configuration.

The temperature dependence of the upper critical field $H_{c2}(T)$, obtained from $M(T,H)$ measurements described above and shown in Fig. 2(b), indicates a much better fit when employing a two-band model than when using the classical models (that are based on assuming a single-band of quasiparticles). The NMR results suggest that a single-band model fits the corresponding data adequately. However, the field-dependent SR results, are best fit using a two-band $(s+s)$-wave gap configuration. Although at first sight the NMR results might seem contradictory, we recall that NMR typically requires high magnetic fields (3 T, in our case), which may easily suppress the smaller superconducting gap and, thus, lead to an apparent single-band scenario.

Also recent DFT calculations [23] seem to support the two-band interpretation since, in the ThIrSi case, they indicate: (i) a mix of isotropic and anisotropic bands near the Fermi level, a requirement for two-band superconductivity, and (ii) large band splittings resulting from spin-orbit coupling (SOC). The combination of multiple bands and large SOC is fully compatible with the two-band model, while it renders the simple single-gap s-wave model unlikely.

However, also the two-gap model runs into theoretical problems. In the two-gap picture, we observe that the SC gap values obtained for ThIrSi are relatively close to each other and the ratio of the relative weights is close to 0.5/0.5. These fit parameters are substantially different from those regarding the sesquicarbides (see Table I), the latter appearing as more clearcut examples of two-gap superconductors. Indeed, contrary to ThIrSi, in the sesquicarbides both NMR and SR data exhibit two-band features. In this sense, it is a still open issue whether ThIrSi is a two-band superconductor.

In general, if the weight of the second gap is relatively small and the gap sizes are not significantly different, this makes it difficult to discriminate between a single- and a two-gap superconductor based on temperature-dependent superconducting properties. For ThIrSi, the weight of the second gap $w = 0.3$ and the gap sizes are quite similar (see Table I). As a consequence, the multigap feature is less evident in the temperature-dependent superfluid density (see Fig. 4). From the analysis of $H_{c2}(T)$ using a two-band model, the derived inter-band and intra-band couplings are $\lambda_{12} = 0.03$ and $\lambda_{11} \sim \lambda_{22} = 0.25$ for ThIrSi. Such an inter-band coupling is much smaller than the intra-band coupling, a circumstance which makes the gaps to open at different electronic bands, less distinguishable compared with other multiband superconductors (see Table I) [47]. However, the underlying multigap SC feature of ThIrSi is reflected in its upper critical fields $H_{c2}(T)$ (see Fig. 2). The measurement of the field-dependent superconducting Gaussian relaxation rate $\sigma_{sc}(H)$ also provides evidence of multiband SC (see Fig. 5, which shows a distinct field response compared to a single-gap superconductor [43, 48]).

While the discrepant SC-gap values remain an open problem, the lack of TRS breaking deduced from ZF-SR, excludes the possibility of spin-triplet- or other non s-wave superconductivity mechanisms in ThIrSi.

IV. CONCLUSION

In summary, we presented the results of an extensive study of the properties of the non-centrosymmetric superconductor ThIrSi, by employing magnetometry, as well as NMR and SR techniques. Experimental data confirm the formation of a nodeless gap configuration in the superconducting state. Nevertheless, data interpretation does not allow for a clear decision whether ThIrSi adopts a single- s or a two-band $(s+s)$ superconducting state. Future experimental and theoretical investigations of similar materials may help to clarify the link between the non-centrosymmetry of the crystal structure and multiband superconductivity. In this respect, DFT calculations show that ThNiSi and ThPtSi have multiple bands near (or crossing) the Fermi level [23] and, hence, are suitable candidate materials to search for multigap superconductivity, once they can be shown to adopt a superconducting state at low temperatures.

ACKNOWLEDGMENTS

This work was supported from the Natural Science Foundation of Shanghai (Grants No. 21ZR1420500 and 21JC1402300), This work was supported by the Natural Science Foundation of Shanghai (Grants No. 21ZR1420500 and 21JC1402300), the Natural Science Foundation of Chongqing (Grant No. CSTB2022NSCQ-MSX1678), the Fundamental Research Funds for the Central Universities, and the Schweizerische Nationalfonds zur Förderung der Wissenschaftlichen Forschung (SNF) (Grants No. 200021_188706 and 206021_139082). Work at Los Alamos was supported by the U.S. Department of Energy, Office of Science, National Quantum Information Science Research Centers, Quantum Science Center. F.B.S. was supported by FAPESP under Grants No. 2016/11565-7 and 2018/20546-1. We acknowledge the allocation of beam time at the Swiss muon source (GPS SR spectrometer).

* Corresponding authors: tshang@phy.ecnu.edu.cn
† tshiroka@phys.ethz.ch

[1] E. Bauer and M. Sigrist, eds., *Non-Centrosymmetric Superconductors*, Lecture Notes in Physics, Vol. 847 (Springer Verlag, Berlin, 2012).
[2] M. Smidman, M. B. Salamon, H. Q. Yuan, and D. F. Agterberg, Superconductivity and spin–orbit coupling in non-centrosymmetric materials: A review, Rep. Prog. Phys. **80**, 036501 (2017).

[3] S. K. Ghosh, M. Smidman, T. Shang, J. F. Annett, A. D. Hillier, J. Quintanilla, and H. Yuan, Recent progress on superconductors with time-reversal symmetry breaking, J. Phys.: Condens. Matter **33**, 033001 (2020).
[4] H. Kim, K. Wang, Y. Nakajima, R. Hu, S. Ziemak, P. Syers, L. Wang, H. Hodovanets, J. D. Denlinger, P. M. R. Brydon, D. F. Agterberg, M. A. Tanatar, R. Prozorov, and J. Paglione, Beyond triplet: Unconventional superconductivity in a spin-3/2 topological semimetal, Sci. Adv. **4**, eaao4513 (2018).
[5] Z. X. Sun, M. Enayat, A. Maldonado, C. Lithgow, E. Yelland, D. C. Peets, A. Yaresko, A. P. Schnyder, and P. Wahl, Dirac surface states and nature of superconductivity in noncentrosymmetric BiPd, Nat. Commun. **6**, 6633 (2015).
[6] M. N. Ali, Q. D. Gibson, T. Klimczuk, and R. J. Cava, Noncentrosymmetric superconductor with a bulk three-dimensional Dirac cone gapped by strong spin-orbit coupling, Phys. Rev. B **89**, 020505(R) (2014).
[7] M. Sato and S. Fujimoto, Topological phases of noncentrosymmetric superconductors: Edge states, Majorana fermions, and non-Abelian statistics, Phys. Rev. B **79**, 094504 (2009).
[8] Y. Tanaka, Y. Mizuno, T. Yokoyama, K. Yada, and M. Sato, Anomalous Andreev bound state in noncentrosymmetric superconductors, Phys. Rev. Lett. **105**, 097002 (2010).
[9] M. Sato and Y. Ando, Topological superconductors: A review, Rep. Prog. Phys. **80**, 076501 (2017).
[10] X.-L. Qi and S.-C. Zhang, Topological insulators and superconductors, Rev. Mod. Phys. **83**, 1057 (2011).
[11] C. Kallin and J. Berlinsky, Chiral superconductors, Rep. Prog. Phys. **79**, 054502 (2016).
[12] A. Shimamura, Y. Furukawa, K. Kumagai, H. Takeya, and K. Hirata, NMR study of noncentrosymmetric superconductor Li_2Pt_3B, Physica C **460–462**, 663 (2007).
[13] T. Shang, W. Xie, J. Z. Zhao, Y. Chen, D. J. Gawryluk, M. Medarde, M. Shi, H. Q. Yuan, E. Pomjakushina, and T. Shiroka, Multigap superconductivity in centrosymmetric and noncentrosymmetric rhenium-boron superconductors, Phys. Rev. B **103**, 184517 (2021).
[14] D. Tay, T. Shang, Y. P. Qi, T. P. Ying, H. Hosono, H.-R. Ott, and T. Shiroka, *s*-wave superconductivity in the noncentrosymmetric W_3Al_2C superconductor: An NMR study, J. Phys.: Condens. Matter **34**, 194005 (2022).
[15] E. Bauer, C. Sekine, U. Sai, P. Rogl, P. K. Biswas, and A. Amato, Absence of time-reversal symmetry breaking in the noncentrosymmetric superconductor Mo_3Al_2C, Phys. Rev. B **90**, 054522 (2014).
[16] T. Shang, D. Tay, H. Su, H. Q. Yuan, and T. Shiroka, Evidence of fully gapped superconductivity in NbReSi: A combined μSR and NMR study, Phys. Rev. B **105**, 144506 (2022).
[17] J. Nagamatsu, N. Nakagawa, T. Muranaka, Y. Zenitani, and J. Akimitsu, Superconductivity at 39 K in magnesium diboride, Nature **410**, 63 (2001).
[18] S. Souma, Y. Machida, T. Sato, T. Takahashi, H. Matsui, S.-C. Wang, H. Ding, A. Kaminski, J. C. Campuzano, S. Sasaki, and K. Kadowaki, The origin of multiple superconducting gaps in MgB_2, Nature **423**, 65 (2003).
[19] A. Harada, S. Akutagawa, Y. Miyamichi, H. Mukuda, Y. Kitaoka, and J. Akimitsu, Multigap superconductivity in Y_2C_3: A ^{13}C-NMR study, J. Phys. Soc. Jpn. **76**, 023704 (2007).
[20] S. Kuroiwa, Y. Saura, J. Akimitsu, M. Hiraishi, M. Miyazaki, K. H. Satoh, S. Takeshita, and R. Kadono, Multigap superconductivity in sesquicarbides La_2C_3 and Y_2C_3, Phys. Rev. Lett. **100**, 097002 (2008).
[21] S. Akutagawa and J. Akimitsu, Superconductivity of Y_2C_3 investigated by specific heat measurement, J. Phys. Soc. Jpn. **76**, 024713 (2007).
[22] T. Ekino, A. Sugimoto, A. M. Gabovich, H. Kinoshita, and J. Akimitsu, Tunneling break-junction measurements of the superconducting gap in Y_2C_3, Physica C **484**, 52 (2013).
[23] A. Ptok, K. Domieracki, K. J. Kapcia, J. Łażewski, P. T. Jochym, M. Sternik, P. Piekarz, and D. Kaczorowski, Electronic and lattice properties of noncentrosymmetric superconductors Th*T*Si (*T*=Co, Ir, Ni, and Pt), Phys. Rev. B **100**, 165130 (2019).
[24] K. Klepp and E. Parthé, *R*PtSi phases (*R* = La, Ce, Pr, Nd, Sm and Gd) with an ordered $ThSi_2$ derivative structure, Acta Crystallogr. B **38**, 1105 (1982).
[25] G. V. Subba Rao, K. Wagner, G. Balakrishnan, J. Janaki, W. Paulus, R. Schöllhorn, V. S. Subramanian, and U. Poppe, Structure and superconductivity studies on ternary equiatomic silicides, MM'Si, Bull. Mater. Sci. **7**, 215 (1985).
[26] W. X. Zhong, W. L. Ng, B. Chevalier, J. Etourneau, and P. Hagenmuller, Structural and electrical properties of new silicides: $ThCo_xSi_{2-x}$ ($0 \leq x \leq 1$) and ThTSi (T = Ni, Pt), Mater. Res. Bull. **20**, 1229 (1985).
[27] B. Chevalier, W. X. Zhong, B. Buffat, J. Etourneau, P. Hagenmuller, P. Lejay, L. Porte, T. M. Duc, M. Besnus, and J. Kappler, Etude de nouveaux supraconducteurs $ThIr_xSi_{2-x}$ ($0 \leq x \leq 1$) par chaleur specifique a basse temperature et spectroscopie XPS, Mater. Res. Bull. **21**, 183 (1986).
[28] T. Shang, S. K. Ghosh, M. Smidman, D. J. Gawryluk, C. Baines, A. Wang, W. Xie, Y. Chen, M. O. Ajeesh, M. Nicklas, E. Pomjakushina, M. Medarde, M. Shi, J. F. Annett, H. Yuan, J. Quintanilla, and T. Shiroka, Spin-triplet superconductivity in Weyl nodal-line semimetals, npj Quantum Mater. **7**, 35 (2022).
[29] A. Suter and B. M. Wojek, Musrfit: A free platform-independent framework for μSR data analysis, Phys. Procedia **30**, 69 (2012).
[30] X. Zhu, H. Yang, L. Fang, G. Mu, and H.-H. Wen, Upper critical field, Hall effect and magnetoresistance in the iron-based layered superconductor $LaFeAsO_{0.9}F_{0.1-\delta}$, Supercond. Sci. Technol. **21**, 105001 (2008).
[31] N. R. Werthamer, E. Helfand, and P. C. Hohenberg, Temperature and purity dependence of the superconducting critical field, H_{c2}. III. Electron spin and spin-orbit effects, Phys. Rev. **147**, 295 (1966).
[32] A. Gurevich, Iron-based superconductors at high magnetic fields, Rep. Prog. Phys **74**, 124501 (2011), and references therein.
[33] K.-H. Müller, G. Fuchs, A. Handstein, K. Nenkov, V. N. Narozhnyi, and D. Eckert, The upper critical field in superconducting MgB_2, J. Alloys Compd. **322**, L10 (2001).
[34] A. Gurevich, S. Patnaik, V. Braccini, K. H. Kim, C. Mielke, X. Song, L. D. Cooley, S. D. Bu, D. M. Kim, J. H. Choi, L. J. Belenky, J. Giencke, M. K. Lee, W. Tian, X. Q. Pan, A. Siri, E. E. Hellstrom, C. B. Eom, and D. C. Larbalestier, Very high upper critical fields in MgB_2 produced by selective tuning of impurity scattering, Supercond. Sci. Technol. **17**, 278 (2004).
[35] Y. Nakajima, H. Hidaka, T. Nakagawa, T. Tamegai, T. Nishizaki, T. Sasaki, and N. Kobayashi, Two-band superconductivity featuring different anisotropies in the ternary iron silicide $Lu_2Fe_3Si_5$, Phys. Rev. B **85**, 174524 (2012).
[36] E. H. Brandt, Properties of the ideal Ginzburg-Landau vortex lattice, Phys. Rev. B **68**, 054506 (2003).
[37] A. Yaouanc and P. D. de Réotier, *Muon Spin Rotation, Relaxation, and Resonance: Applications to Condensed Matter* (Oxford University Press, Oxford, 2011).
[38] A. Amato, Heavy-fermion systems studied by μSR technique, Rev. Mod. Phys. **69**, 1119 (1997).
[39] S. J. Blundell, Spin-polarized muons in condensed matter physics, Contemp. Phys. **40**, 175 (1999).
[40] W. Barford and J. M. F. Gunn, The theory of the measurement of the London penetration depth in uniaxial type-II superconductors by muon spin rotation, Physica C **156**, 515 (1988).
[41] M. Tinkham, *Introduction to Superconductivity*, 2nd ed. (Dover Publications, Mineola, NY, 1996).
[42] A. Carrington and F. Manzano, Magnetic penetration depth of MgB_2, Physica C **385**, 205 (2003).
[43] T. Shang, W. Xie, D. J. Gawryluk, R. Khasanov, J. Z. Zhao, M. Medarde, M. Shi, H. Q. Yuan, E. Pomjakushina,

and T. Shiroka, Multigap superconductivity in the Mo_5PB_2 boron–phosphorus compound, New J. Phys. **22**, 093016 (2020).

[44] S. Serventi, G. Allodi, R. De Renzi, G. Guidi, L. Romanò, P. Manfrinetti, A. Palenzona, C. Niedermayer, A. Amato, and C. Baines, Effect of two gaps on the flux-lattice internal field distribution: Evidence of two length scales in $Mg_{1-x}Al_xB_2$ from μSR, Phys. Rev. Lett. **93**, 217003 (2004).

[45] R. Khasanov, A. Amato, P. K. Biswas, H. Luetkens, N. D. Zhigadlo, and B. Batlogg, $SrPt_3P$: A two-band single-gap superconductor, Phys. Rev. B **90**, 140507(R) (2014).

[46] D. E. MacLaughlin, Magnetic resonance in the superconducting state, in *Solid State Physics*, Vol. 31, edited by H. Ehrenreich, F. Seitz, and D. Turnbull (Academic Press, San Diego, 1976) pp. 1–69, and references therein; R. E. Walstedt, *The NMR Probe of High-T_c Materials*, Springer Tracts in Modern Physics, Vol. 228 (Springer Verlag, Heidelberg, 2008).

[47] V. G. Kogan, C. Martin, and R. Prozorov, Superfluid density and specific heat within a self-consistent scheme for a two-band superconductor, Phys. Rev. B **80**, 014507 (2009).

[48] T. Shang, A. Amon, D. Kasinathan, W. Xie, M. Bobnar, Y. Chen, A. Wang, M. Shi, M. Medarde, H. Q. Yuan, and T. Shiroka, Enhanced T_c and multiband superconductivity in the fully-gapped $ReBe_{22}$ superconductor, New J. Phys. **21**, 073034 (2019).